4 CHAPTER

OPTIMIZATION TECHNIQUES BASED BI-STABLE DYNAMIC STOCHASTIC RESONANCE FOR THE ENHANCEMENT OF MRI DATA

Objectives of the Chapter

- *Implementation of MO-PSO based quartic bi-stable model of DSR*
- *Implementation of Bat optimization based neuron model of DSR*
- *Implementation of MO-PSO based cascaded model of DSR*
- *A comparative study of considered DSR models*

Abstract

Dynamic stochastic resonance (DSR) is the technique that utilizes the noise to enhance the contrast and hence, this technique has the ability to encounter the possibility of noise amplification in the process of contrast enhancement of MRI data. The quality of the processed MRI data depends on the parameter values of DSR models, hence, to obtain the optimum value of these parameters is an essential prerequisite. The optimization techniques such as: (i) Multi-Objective Particle Swarm Optimization (MO-PSO) and (ii) multi-objective

bat optimization (MO-Bat) have been used to tune the DSR parameters associated with the different models for the maximization of two image quality measures. Further, the maximization of another image quality measure helps to obtain the optimum enhanced image from the Pareto fronts solution. The present chapter implements: (i) Quartic bi-stable model, (ii) Neuron model and (iii) Cascaded model of DSR. The proposed algorithms based on these three models have been tested on simulated MRI data for validation and comparison. Further, the implementation of algorithms on real MRI data has been found valuable in the diagnosis of lacunar infarct, edema, mesial temporal sclerosis, etc.

4.1 Introduction

Magnetic Resonance Imaging (MRI) has advantages over other medical imaging modalities in terms of superior contrast resolution of soft tissues [144, 145]. The MRI sequences such as T1, T2, diffusion-weighted imaging (DWI) and fluid attenuated inversion recovery (FLAIR) are beneficial in analysis and diagnosis of various neuropathologies and anatomical structure study of the brain. T1 weighted sequence closely approximates the macroscopical appearances of the tissues and obtains morphological information. T2 weighted sequence is generally used to identify the edema in the soft tissues. DWI is an isotropic T2 weighted map, usually has application in the diagnosis of acute pathology such as ischemic stroke, cellular tumor, whereas FLAIR sequence removes the effect of fluid and identifies the subtle changes at the periphery of the hemispheres and in the periventricular region near to cerebrospinal fluid. More or less image data obtained from all sequences of MRI suffer from low contrast and low signal to noise ratio (SNR), which may lead to poor readability and hence may affect the quality of diagnosis. Hence, these images need to be de-noised and contrast-enhanced for better readability.

Previously, noise estimation followed by filtering of MRI data has been performed using LMMSE approach [27, 119] and iterative bilateral filter approach [125]. These methods are very efficient and popular for de-noise the MRI data. Other than the filtering approaches, some algorithms have been developed to improve the tissue contrast of MRI data. The adaptive fractional differential algorithm applied to different modalities of medical imaging to enhance the contrast and information entropy of image [57]. Recently, the information preserving approach has been adapted to enhance the MRI data for better detection of benign brain tumor [146]. The majority of these algorithms underwent a trade-off between noise reduction and the tissue-selective contrast enhancement of the image.

The recent trends in DSR approaches have shown remarkable performance for the enhancement of MRI data. This system demonstrates a nonlinear phenomenon, which is useful for the enhancement of the low contrast images. The nonlinear dynamics such as quartic bistable model [147], potential neuron model [148] and Hodgkin–Huxley neuron model [149] has shown the properties of stochastic resonance, and hence known as DSR. The quartic bistable is the most studied DSR model for the application of image enhancement. Previously, the quartic bistable model used Fourier transform and found valuable for tissue-specific diagnosing of brain lesions in MRI [54]. The DSR based wavelet-transform improved the appearance of ultrasound images of the breast, abdomen, veins and vascular arteries [109]. However, the drawbacks of these methods are the non-optimum selection of DSR parameters values, which resist DSR to produce best image enhancement.

In the process of enhancement, the different models of DSR may address the different enhancement quality measures of MRI data is the main idea behind the exploration of other DSR models such as neuron bi-stable model. Previously, in best of knowledge, none of the

studies has considered potential neuron model of stochastic resonance for the enhancement of the image data, maybe because of unavailability of an approach that can tune or automatically obtained the parameter for the enhancement of MRI data. There are three main contributions of this chapter given as follows:

The present study has suggested to obtain optimum enhanced MRI data with the help of adaptive selection of DSR parameters for (i) quartic bi-stable model, where multi-objective PSO searches the appropriate DSR parameters, (ii) potential neuron model, in this case multi-objective Bat searches the appropriate DSR parameters and (iii) cascaded model uses the multi-objective PSO to obtained best enhanced MRI data.

4.2 Dynamic stochastic resonance

DSR was first examined for the probable description of the periodicity of Earth's ice ages where normal climate and mostly ice-covered state is modelled as two metastable states divided by an energy barrier [99]. Recent studies have shown that DSR helps to amplify a weak signal with the aid of an appropriate level of noise in the existence of the nonlinear system. The added noise to the weak signal must be high enough so that together they can cross the threshold and change the state of a nonlinear system whereas the high amount of noise may lead to oscillations between two states and degrades the performance. Further, the parameter associated with the system can control the threshold level and hence the appropriate choice of these parameters enhance the performance, i.e., enhancement of MRI data. The study has considered two DSR models and the cascaded of these models given as follows: (i) quartic bi-stable model, and (ii) neuron bi-stable model.

4.2.1 Quartic Bistable Model

The quartic bistable model is the most popular model of DSR. The dynamic equation of motion of a Brownian particle given as follows [150]:

$$\frac{d}{dt}\,x(t) = -\,\frac{d}{dt}\,U\,(x,t)\;+\;s(t)\;+\;n(t) \tag{4.1}$$

where $U\,(x,t)$ represents the dynamics of quartic potential, $s\,(t)$ is the input signal and $n\,(t)$ is the noise added to the system. The quartic potential $U\,(x,t)$ defined as [107, 147]:

$$U(x,t) = -\,a\,\frac{x^2}{2} + \,b\,\frac{x^4}{4} \tag{4.2}$$

where $a > 0$ and $b > 0$ are the parameters associated with doublethe well quartic bistable system. There is two stable states in this double well system at points: $x_m = \pm\sqrt{\frac{a}{b}}$ and one metastable state at $x = 0$. As shown in Fig. 4.1. (c, d), the Brownian particle need to cross potential bathe rrier $\Delta U = \frac{a^2}{4\,b}$ to attain one stable state from another, which helps to achieve enhanced information. The final dynamic equation for quartic bi-stable model based DSR is given as follows:

$$\frac{d}{dt}\,x(t) = a\,x - b\,x^3 \;+\; input \tag{4.3}$$

The term $input$ given in above equation represents the Discrete Cosine Transform (DCT) of input MRI data $I(i,j)$. The DCT of $I(i,j)$ having the size $M \times N$ is obtained as follows:

$$I(k_i,k_j) = \left(\frac{2}{N}\right)^{\frac{1}{2}}\left(\frac{2}{M}\right)^{\frac{1}{2}}\sum_{i=0}^{N-1}\sum_{j=0}^{M-1}\Lambda\,(i)\Lambda\,(j)I(i,j)\cos\frac{(2i+1)k_i\pi}{2M}\cos\frac{(2j+1)\,k_j\,\pi}{2N} \tag{4.4}$$

$$where, \Lambda\,(i) = \begin{cases} \dfrac{1}{\sqrt{2}} & for\ \xi = 0 \\ 1 & otherwise \end{cases}$$

The study chooses the DCT, as it has the spectral separation property that helps to improve the features of the image as it processes the various frequency components independently. Now, the image $I(k_i, k_j)$ shown in Equ.4.4 serves as $input$ in Equ.4.3.

$$x(n_q + 1) = x(n_q) + k\,[a\,x(n_q) - b\,x^3(n_q) + input] \tag{4.5}$$

Optimization algorithm searches the position of the particle, i.e. dynamic parameters a, b, n_q of the quartic bistable model given in Equ.4.5 for the objective of maximum contrast enhancement factor (CEF) [54] and Mean Opinion Score (MOS) [151] of the image.

4.2.2 Potential Neuron Model

The motion of a Brownian particle in the presence of signal and noise defined by the dynamic equation of stochastic resonance is given as follows [148]:

$$\frac{d}{dt}x(t) = -\frac{d}{dx}U(x,t) + \epsilon\,(\sin\omega t) + n_a(t) \tag{4.6}$$

where x is a state variable expressing the firing rate, $U(x,t)$ is neuron potential, $n_a(t)$ is the additive noise and ϵ is the small amplitude of signal. The potential $U(x,t)$ of neuron is defined as follows [152]:

$$U(x,t) = \frac{x^2}{2} - \lambda(t)\,log_e(\cosh x) \tag{4.7}$$

where $\lambda(t) = \lambda_0 + n_m(t)$, λ_0 constant and $n_m(t)$ is multiplicative noise. Fig. 4.1. (a, b), shows the potential curve for this model, where the Brownian particle changes its position from one stable state to another. Now, substitute the value of $U(x,t)$ from Equ.4.7 in Equ.4.8

$$\frac{d}{dt}x(t) = -x + \lambda(t)\tanh x + input \tag{4.8}$$

where '*input*' is considered as the DCT of low contrast input MRI data, as given in Equation (4.4). The system will remain bistable if $\epsilon < \Delta U$, however, in absence of noise the

switching will not occur. The dynamics shown in Equ.4.7 has been modified for better image enhancement suggested as follows:

$$\frac{d}{dt}x(t) = -w_f x + \lambda\,(\mathrm{t})\tanh x + input \qquad (4.9)$$

$where\ w_f$ is a modification factor. The modification factor helps to increase the potential difference ΔU of the system, and hence increases the moving distance for Brownian particle. In presence of same input and noise, the noise can be effectively utilize if a Brownian particle has more moving distance, and hence, better enhancement can be achieved [106].

The Equ.4.9 has discretized in the step size of k using Euler-Maruyama's method [153]. The final cascaded DSR is given as follows:

$$x(n_n + 1) = \left(1 - w_f\, k\right) x(n_n) + k\,[\lambda_0 \tanh x(n_n) + input] \qquad (4.10)$$

Optimization algorithm searches the position of particle in the form of the parameters λ_0, n_n given in Equ.4.9 for the objective of maximum contrast enhancement factor (CEF) [54] and mean opinion score (MOS) [154] of the image. The coefficients of the transformed image were processed with modified ($w_f = 0.45$) neuron model of DSR.

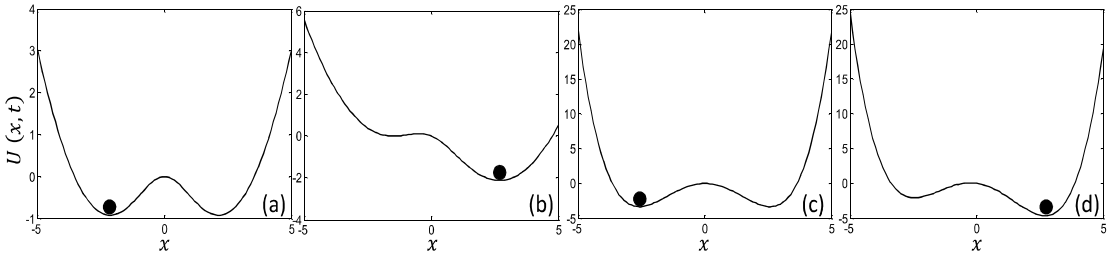

Figure 4-1: Potential function curves for (a) unmodulated potential neuron model for $\lambda = 2.2$, (b) modulated potential neuron model for $\lambda = 2.2$, $t = 0$ and $n_a = 0.5$ (c) unmodulated quartic bistable system for $a = 2, b = 0.3$ and (d) modulated quartic bistable system for $a = 2, b = 0.3$, $t = 0$ and $n = 0.5$

4.2.3 Cascaded DSR

Further, the cascaded DSR, the energy of high-frequency signals efficiently moves towards low frequency [155]. Hence, the energy of low-frequency signal rises, and there is the decrease in the high-frequency noise components. In this way, the cascaded DSR can remove the high-frequency ingredients and increases the signal strength. The present study cascades two different non-linear models of DSR and optimizes its dynamics for the enhancement of low contrast MRI data. The dynamic equation of modified neuron model is given as follows:

$$\dot{x} = -w_f\, x + \lambda_0 \tanh x \; + input \tag{4.11}$$

The pixel values of the transformed image are discrete in nature. Hence, this differential needs to convert in the discrete domain. The Equ.4.11 discretized in k steps using Euler-Maruyama's method [153]. The dynamics of modified neuron model is given as follows:

$$x(n_n + 1) = \left(1 - w_f\, k\right) x(n_n) + k\, [\lambda_0 \tanh x(n_n) + input] \tag{4.12}$$

After a specific number of DSR iterations, the $x(n_n + 1)$ gets update, and stored in an output variable say, $input'$. This output variable replaces $s(t) + n(t)$ given in Equ.4.3, which is the dynamic model of the quartic bi-stable system. Hence, the new equation can be rewritten as:

$$\dot{x} = a\, x - b\, x^3 \; + input' \tag{4.13}$$

The Equ.4.13 has discretized in the step size of k using Euler-Maruyama's method [153]. The final cascaded DSR is given as follows:

$$x\left(n_q + 1\right) = x\left(n_q\right) + k\, [a\, x(n_q) - b\, x^3(n_q) + input'] \tag{4.14}$$

Optimization algorithm searches the position of particle in the form of the parameters λ_0, n_n given in Equ.4.12, and the parameters a, b, n_q given in Equ.4.14 for the objective of maximum contrast enhancement factor (CEF) [54] and universal image quality (UIQ) [151] of the image.

4.3 Optimization techniques

Two evolutionary computation techniques have been considered to optimize the image quality using bi-stable DSR models, these techniques are (i) MO-PSO, and (ii) MO-Bat optimization. The dynamic parameters of quartic bistable DSR model have been tuned with the help of MO-PSO, dynamic parameters of modified neuron model have been tuned with MO-Bat optimization whereas dynamic parameters of cascaded DSR model have been tuned with the MO-PSO algorithm.

4.3.1 Particle Swarm Optimization

Particle Swarm Optimization (PSO) is an evolutionary search algorithm developed by Eberhart and Kennedy in 1995 [94]. The computation process of PSO is inspired by the social behavior of bird flocks. The population in PSO is called the particles, and these particles grow over the iterations to find the optimum value within the range of search space. Each particle has a velocity and position vector that facilities it to move over the search space in search of the optimal solution. These particles keep track of their locations in the hyperspace, and these locations are related to the solution (fitness). The fitness of a particle is the value of the objective function at the current position of the particle. Personal best (pbest) is the best location of each particle. Global best (gbest) is the best performance of the population (all the particles) obtained so far. If the search space of PSO is D-dimensional, the position of k^{th} particle of the population can be represented

by $X_k = (x_{k1}, x_{k2} \ldots, x_{kD})$. The velocity and best previous position of this particle can be represented by $V_k = (v_{k1}, v_{k2} \ldots, v_{kD})$ and $P_k = (p_{k1}, p_{k2} \ldots, p_{kD})$ respectively. The best particle in the population is define as g. The velocity of k^{th} particle in D-dimension (v_{kD}) is determine with the help of additive influence of this particle in previous generations which is called momentum, individual weighting of its distance from p_{kD} is called cognitive and its distance from g_D is called social component. There are two acceleration coefficients c_2 and c_1 determine the impact of the social component and cognitive component respectively.

$$v_{kD}^{n+1} = w \times v_{kD}^{n} + c_1 \times r_1 \times (p_{kD} - x_{kD}^{n}) + c_2 \times r_2 \times (g_D - x_{kD}^{n}) \quad (4.15)$$

The position of the particle at n^{th} iteration is x_{kD}^{n}, which is updated as follows:

$$x_{kD}^{n+1} = x_{kD}^{n} + v_{kD}^{n+1} \quad (4.16)$$

$where\ r_1$, r_2 are the random numbers ranged between 0 and 1 and w is the inertia weight. The velocity and position of particles are keep updating and evaluating the fitness until the expected convergence is met. The controlling parameters chosen for the experiment are given in Table 4-1.

Table 4-1: Controlling parameters of multi-objective PSO

Parameter	Quartic bi-stable DSR	modified cascaded DSR
Maximum number of iterations	25	25
Population size	15	15
c_1, c_2	1.2	1.2
w_{min}, w_{max}	0.4, 0.9	0.4, 0.9
Fitness Functions	$CEF,\ MOS$	$CEF,\ UIQ$
Variables	$a, b, and\ n_q$	$a, b, \lambda_0\ n_q\ and\ n_n$

4.3.2 Bat Algorithm

Optimization is a process that gives an optimal solution for one or more than one objective functions with the given constraints. Yang et al. proposed a powerful algorithm namely Bat algorithm (BA) inspired by echolocation property of microbats [156]. Generalized rules for BA are: (i) Bats use echolocation property to sense the distance, and they know the difference between food and the background barriers. (ii) Bats fly randomly with the velocity of v_i from position x_i, fixed frequency f_{min}, variable wavelength λ and loudness A_0 to search for the food. (iii) Bats can vary their loudness from maximum A_0 to minimum A_{min}. Algorithm initializes with bat population and these bats evolve over the generations to find the optima. Each bat is randomly initialized with the frequency range of $[f_{min}\ \ f_{max}]$, where f_{min} and f_{max} are the minimum and maximum frequency values respectively. The velocity v_i corresponding to the i^{th} bat is affected by its predefined frequency f_i. Moving towards the solution x_i^t, the velocity v_i^t of the bat in time steps t updates as:

$$f_i = f_{min} + (f_{max} - f_{min})\,\beta, \tag{4.17}$$

$$v_i^t = v_i^{t-1} + (x_i^t - x_*)f_i, \tag{4.18}$$

$$x_i^t = x_i^{t-1} + v_i^t, \tag{4.19}$$

where $\beta \in [0\ \ 1]$ is a random vector and x_* is a current global best solution among all n bats. The new solution for each bat in order to improve local search capability of the algorithm is:

$$x_{new} = x_{old} + \epsilon\, A^t\,, \tag{4.20}$$

where ϵ is randomly generated value ranging from [-1 1] and A^t is the average loudness value of all the bats. As the iterations proceed, the values of loudness A_i and pulse emission

rate r_i are updated. Usually, the loudness decreases whereas the pulse emission rate increases as follows:

$$A_i^{t+1} = \alpha A_i^t \quad (4.21)$$

$$r_i^{t+1} = r_i^0(1 - e^{\Upsilon t}) \quad (4.22)$$

where α and Υ are the constraints values of these parameters for present application are shown in Table 4-2.

Table 4-2: Controlling parameters for MO-BA

Parameter	Modified neuron model
Maximum number of iterations	22
Size of population n	10
Loudness α	0.25
Pulse rate Υ	0.50
Frequency	0 – 2
Fitness Function	F, MOS
Optimization variables	η_0 and n

4.3.3 Multi-objective optimization

Multi-objective optimization optimizes more than one objective functions and gives a set of optimal solutions. For a multi-objective optimization problem, any two solutions s_1 and s_2 can have one of two possibilities: none dominates the other or one dominates the other. These two conditions are given below:

$$\forall\, i \in \{1, 2, \ldots, N_{obj}\} : f_i(s_1) \leq f_i(s_2)$$

$$\exists j \in \{1, 2, \ldots, N_{obj}\} : f_j(s_1) < f_j(s_2)$$

The solution s_1 does not dominate solution s_2 in case of violation of any above condition. The solutions that are non-dominated in the search space are called as Pareto-optimal solutions. The Pareto front surfaces are the set of the Pareto-optimal solution, which results in a set of near optimal trade-off values [157].

4.4 Material and Methods

The proposed algorithm has been applied to enhance T1 weighted, EPI (Eco planner imaging) T2 weighted, FLAIR and DWI (b=1000) obtained from 1.5 T Magnetom Avanto (Version BV-I7A; Siemens Medical System, Erlangen, Germany) system in DICOM format. We selected image slices that had the maximum cross-section of the region of interest. The acquisition of T1 weighted sequence used the following parameters setting: slice thickness 5 mm, repetition time (TR) 550 ms, echo time (TE) 8.4 ms, flip angle (FA) 90° and field of view (FOV) 175 × 230 mm. Test 1 and Test 8 are T1 weighted sequences. DWI sequence at b = 1000 and T2 weighted sequence at b = 0 used the following parameters setting: slice thickness 5 mm, TR 3000 ms, TE 89 ms, FA 90° and FOV 229 × 229 mm. The acquisition of FLAIR weighted sequence used the following parameters setting: slice thickness 5 mm, TR 9000 ms, TE 89 ms, inversion time (TI) 2500, FA 150° and FOV 201 × 230 mm. Institute ethical committee of IMS BHU, Varanasi, cleared the study (No.: ECR/526/Inst/UP/2014).

4.4.1 Fitness functions used in the study

4.4.1.1 Maximization of the contrast enhancement factor

Contrast enhancement factor increases to one, as the contrast of output image started to improve over the input image. The value of CEF can be achieved by computing the ratio of post enhancement value of image Q_B and pre enhancement value of the image Q_A.

$$CEF = \frac{Q_B}{Q_A} \tag{4.23}$$

The descriptor for an image quality Q defined as the ratio of variance (σ^2) and mean (μ) of the pixel intensity of image:

$$Q = \frac{\sigma^2}{\mu}$$

where σ is standard deviation and μ is the mean of the image.

4.4.1.2 Maximization of UIQ

Previously, Z. Wang et al. define the image quality measure known as Universal image quality measure (UIQ) index [151], which depends on loss of correlation, contrast distortion and luminance distortion. The range of UIQ is -1 to 1, where 1 represents the best image quality. Assume I_A and I_B are pre and post enhancement images. The UIQ is defined as follows:

$$UIQ = \frac{4\,\sigma_{I_A I_B}\,\overline{I_A}\,\overline{I_B}}{(\sigma_{I_A}{}^2 + \sigma_{I_B}{}^2)[(\overline{I_A})^2 + (\overline{I_B})^2]} \tag{4.24}$$

where $\overline{I_A} = \frac{1}{N}\sum_{i=1}^{N} I_{A_i}$, $\overline{I_B} = \frac{1}{N}\sum_{i=1}^{N} I_{B_i}$, $\sigma_{I_A}{}^2 = \frac{1}{N-1}\sum_{i=1}^{N}(I_{A_i} - \overline{I_A})^2$,

$\sigma_{I_B}{}^2 = \frac{1}{N-1}\sum_{i=1}^{N}(I_{B_i} - \overline{I_B})^2$ and $\sigma_{I_A I_B} = \frac{1}{N-1}\sum_{i=1}^{N}(I_{A_i} - \overline{I_A})\,(I_{B_i} - \overline{I_B})$.

4.4.1.3 Maximization of the mean opinion score (MOS)

The equation of quality assessment model is given as follows:

$$S = \alpha + \beta\, B^{\Upsilon_1} A^{\Upsilon_2} Z^{\Upsilon_3} \tag{4.25}$$

where $\alpha, \beta, \Upsilon_3, \Upsilon_3, \Upsilon_3$ are the model parameters, which were described as: $\alpha = -245.9$, $\beta = 261.9$, $\Upsilon_1 = -0.0240$, $\Upsilon_2 = 0.0160$ and $\Upsilon_3 = 0.0064$ [158]. The evaluation score MOS is derived from:

$$MOS = \frac{4}{1+\exp[-1.0217\,(S-3)]} + 1 \tag{4.26}$$

4.4.2 Selection of the dominant solution from Pareto fronts

The multi-objective optimization results in the set of non-dominant solutions. Each solution represents the different enhancement of MRI data. This study defines the selection criterion to select the best solution among non-dominant solution is based on the maximization of another image quality measure, i.e., Anisotropy.

The image Anisotropy calculates the variances in the directional entropy to evaluate the image quality [131]. The local entropy of every pixel in an image is obtained with the help of Renyi entropy. The discrete space-frequency distribution of Renyi entropy $P[n,k]$ is given as follows:

$$R_\alpha = \frac{1}{1-\alpha} log_2 \left(\sum_n \sum_k P^\alpha[n,k]\right) \quad (4.27)$$

where n and k are the spatial and frequency variables, value the of $\alpha \geq 2$ recommended for space-frequency distribution [159]. Further, the information of special-frequency of an image expressed using Pseudo-Wigner distribution (PWD) method [160]. The PWD has been calculated over N data values placed at position n, followed by quantum normalization and denoted with probability distribution $\breve{P}_n$. The Renyi entropy calculated for n position defined as follows:

$$R_3[n] = \frac{1}{2} log_2\left(\sum_{k=1}^{N} \breve{P}_n^3[k]\right) \quad (4.28)$$

The value of entropy for every pixel of an image $R_3[n,\theta_L]$, where θ_L represents L orientations to measure the entropy. The expected value is calculated as follows:

$$\bar{R}[\theta_L] = \sum_n R_3[n,\theta_L]/M \quad (4.29)$$

where M represents size the of the image. The expected value of the entropy measured at angles $0^{\circ}, 30^{\circ}, 60^{\circ}, 90^{\circ}, 120^{\circ}$ and 150°. Finally, the variance $(\sigma(t))$ of expected value at these orientations is known as Anisotropy of the image.

$$\sigma(t) = \sqrt{\sum_{s=1}^{S}(\mu - \bar{R}\ (\theta_L))^2 / L} \qquad (4.30)$$

where μ is the mean value of $\bar{R}[\theta_L]$.

4.4.3 Constraints on variables

4.4.3.1 Choice of bistability parameter a

It is vital to maintain bistability of the double well system, for this a should be restricted by upper limit as: $a \leq a^{max}$ and the lower limit to $a \geq a^{min} > 0$, which depends on the value of b.

4.4.3.2 Choice of bistability parameter b

The restoring force expressed in terms of gradient of the bistable potential, the maximum restoring force for which double well system will remain stable:

$$R = -\frac{d}{dx}U(x) = -a\,x + b\,x^3$$

$$\frac{d}{dx}R = -a + 3\,b\,x^2 = 0$$

At $x = \sqrt{a/3\,b}$ the maximum value of restoring force will be $R = \sqrt{4\,a^3/27\,b}$ and the condition to obtain maximum signal is [161]:

$$b < \sqrt{4\,a^3/27}$$

4.4.3.3 Choice of number of iterations

As shown in Equ.4.14 output image formation obtained by constructing a matrix using x, which is calculated after each iteration, hence, F and MOS are greatly affected by n. Number of iterations should be $1 < n \leq n^{max}$, $where\ n^{max}$ depends on the step size k of the iterative equation.

4.5 Results and Discussion

4.5.1 Optimized quartic bi-stable model of DSR

The proposed MO-PSO based DSR technique is dealing with two competitive objectives F and MOS using the Pareto front as shown in Fig. 4.2. The red circles shows the near optimal solutions, reflecting the trade-off values of *CEF* and MOS. The images constructing for near optimal solutions were examined by the two experienced radiologist and most of the time the final agreement image was found which is represented by red circles near to the origin, i.e. both objective functions are almost equally important. The proposed algorithm is tested on 40 DW-MR images.

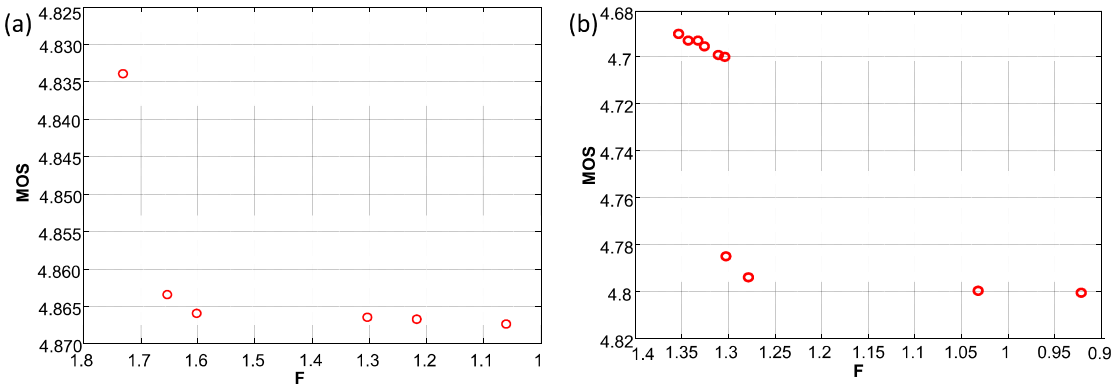

Figure 4-2: Pareto front surface of F and MOS for (a) Test 1 and (b) Test 2 images obtained using MO-PSO

Case I: Fig.4.3 (a) is an echo planar image (EPI) with diffusion weighting (b = 1000) in case of stroke. In the input image, the edema is seen involving the cortex of the left temporal lobe. However, the same also appears to be involving the subcortical white matter (WM) and U-

fibers. The processed output image shown in Fig. 4.3 (b) and its pseudo color image is shown in Fig. 4.3 (f), where the subcortical WM and U-fibers are seem to be spread with the edema being only localized in the gyral/cortical location. This helps in confirming the suspicious that edema is purely cytotoxic in nature and is not associated with any vasogenic component, which would have been seen as spreading edema along WM tracts.

Case II: Fig. 4.3 (c) is an EPI image with no diffusion weighting (b=0) in a case of suspected perinatal brain hypoxia. No features suspicious of hypoxia could be noted. As compare to input image, the differentiation of gray and white matter is better appreciated in the processed output image shown in Fig. 4.3 (d) and its pseudo color image is shown in Fig. 4.3 (h). Note that the terminal zone of myelination is very well seen in the processed image shown in Fig. 4.3 (d), which is crucial in ruling out the possibility of periventricular leukomalacia.

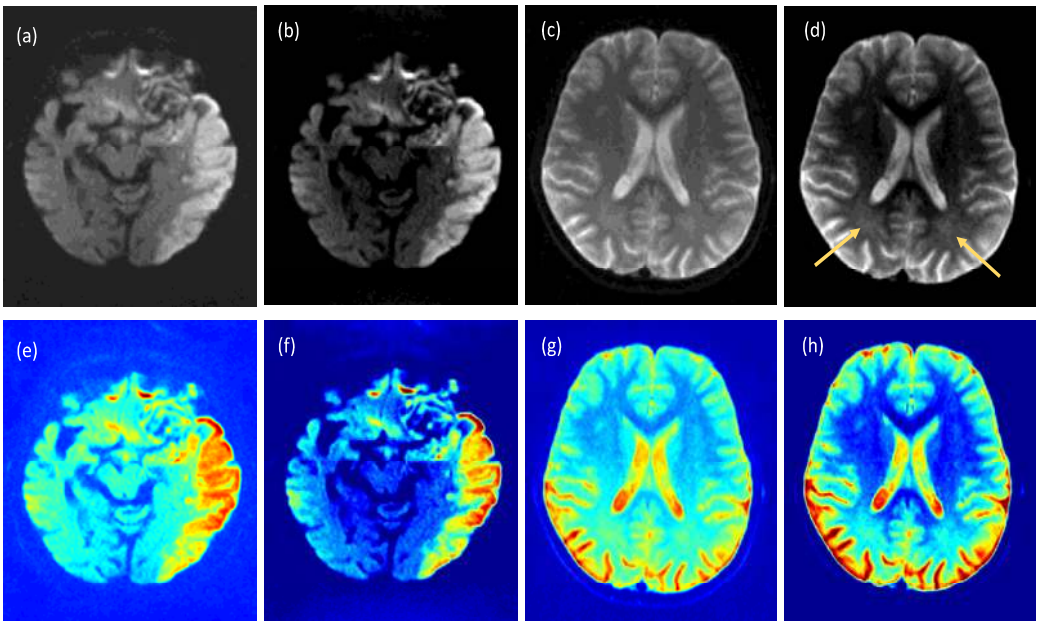

Figure 4-3: Original images (first row) and pseudocolor images (second row) of abnormal and healthy subjects (a) input isotropic DW image (b = 1000 sec/mm2; repetition time (msec)/echo time (msec) = 3,000/89; matrix, 192 × 192; field of view =

250 × 250 mm, section thickness = 5 mm) (c) input isotropic T2 weighted image (b = 0 sec/mm2; repetition time (msec)/echo time (msec) = 3,000/89; matrix, 192 × 192; field of view = 229 × 229 mm, section thickness = 5 mm), and (b, d) proposed algorithm

4.5.1.1 Comparative study

The output images of various existing techniques are shown for Test 3 and Test 4 respectively in Fig. 4.4 and Fig. 4.5. Proposed algorithm is compared to Single-Scale Retinex [162], Histogram Equalization (HE) [163], Contrast Limited Adaptive Histogram Equalization (CLAHE) [164], Gamma correction [163] and Photoshop methods. For Gamma correction, the values of Gamma chosen above and below to one ($\Upsilon = 1.2$ *and* $\Upsilon = 0.9$) and auto contrast of Adobe Photoshop 7 was used for comparison since the proposed technique is also an automatic enhancement technique. The image quality is quantified in terms of F, MOS and perceptual quality metric (PQM) [158]. PQM should be close to 10 for a good perceptual quality image [165].

The image shown in Fig. 4.4 (a) is a T2 weighted EPI with no diffusion weighting of an aging brain. Fig. 4.4 (b) is the SSR processed image that gives an unrealistic look and introduced blur, the differentiation of gray and white matter (GM-WM) is completely lost. Fig. 4.4 (c) shows the histogram equalized image where periventricular demyelination are hard to recognize and artifacts appeared on the image. CLAHE has produced better contrast image in compared to other existing techniques in Fig. 4.4 (d), but appears susceptible to noise. Gamma correction results oversaturated the image as shown in Fig. 4.4 (e), where periventricular demyelination disappeared for $\Upsilon = 1.2$, however, for $\Upsilon = 0.9$ obtained image is informative but suffered from lack of contrast as shown in Fig. 4.4 (f). Image enhancement using Photoshop is visually better than CLAHE, however, produced a low contrast image. Fig. 4.4 (g) shows the image obtained using the proposed method, where GM-WM

differentiation is visualized better, and the areas of periventricular demyelination are visualizing better in comparison to other enhancement methods.

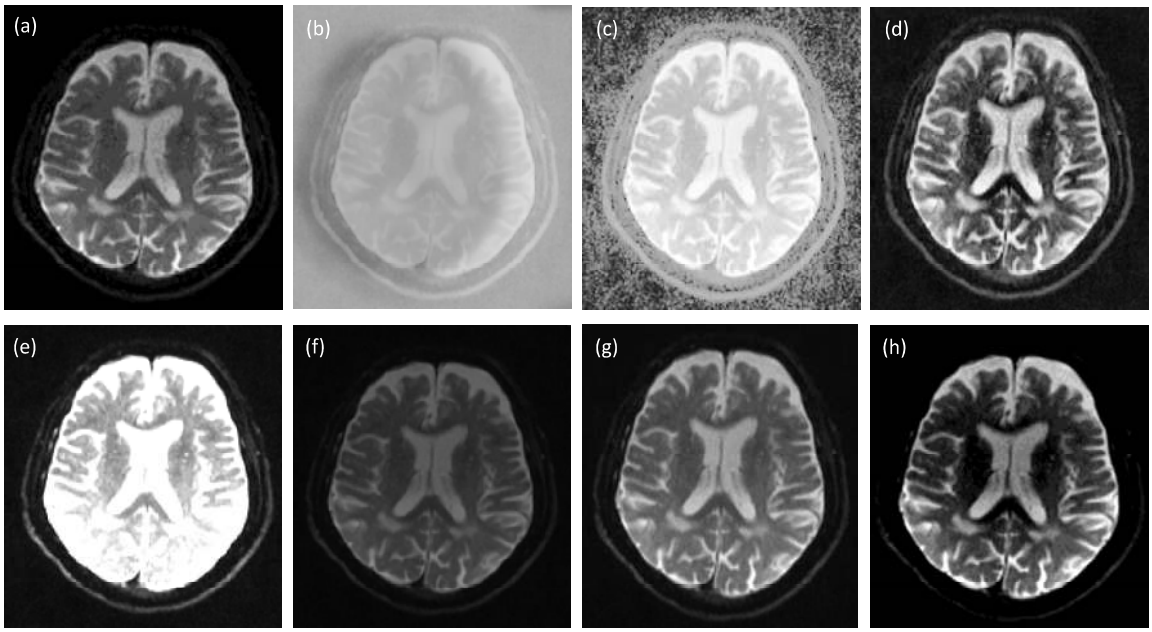

Figure 4-4: Comparative enhancement results of Test 3 (a) input isotropic T2 image (b = 0 sec/mm2; repetition time (msec)/echo time (msec) = 3,000/89; matrix, 192 × 192; field of view = 229 × 229 mm, section thickness = 5 mm), image processed using (b) SSR, (c) HE, (d) CLAHE, (e) Gamma (1.2), (f) Gamma (0.9), (g) Photoshop, and (h) proposed algorithm

Fig. 4.5 (a) is a case of EPI image with diffusion weighting (b=1000) of stroke in cerebral artery territory. The WM edema is visualizing clearer in the processed image shown in Fig. 4.5 (h) that confirms the possibility of sub-acute infract. Similarly, the EPI image with diffusion weighting (b=1000) in case of encephalocele shown in Fig. 4.6 (a). The better GM-WM differentiation, cystic clearing noted in the image using the proposed algorithm as shown in Fig. 4.6 (h) then the other conventional methods, confirming the presence of brain tissue within the cystic diverticulum (shown by the arrow). On the other hand, the conventional methods failed to produce better differentiation of GM-WM in comparison to

the image produced using the proposed algorithm. Table 4-3 shows the quantitative performances of algorithms of Test 3, Test 4 and Test 5 images.

The standard LMMSE based de-noising method [43] followed by conventional enhancement methods are compared with the proposed MO-PSO optimized DSR algorithm. Table 4-4 shows that proposed method has obtained the highest value of CEF in comparison to other techniques for Test 3 and Test 4 images (input test images respectively shown in Fig. 4.4 (a) and Fig. 4.5 (a)). In case of Test 4 image, the filtrating is followed by Gamma correction technique ($\Upsilon = 1.1$) has slightly edge on the proposed algorithm with highest *CEF* however, cost a lot PQM. Further, the proposed algorithm has been tested on 40 DW-MR images and obtained highest mean *CEF* and best mean PQM in comparison to other techniques. The mean PQM obtained by the proposed algorithm is 9.508, which is closer to 10 in comparison to the mean PQM (10.604) of input images.

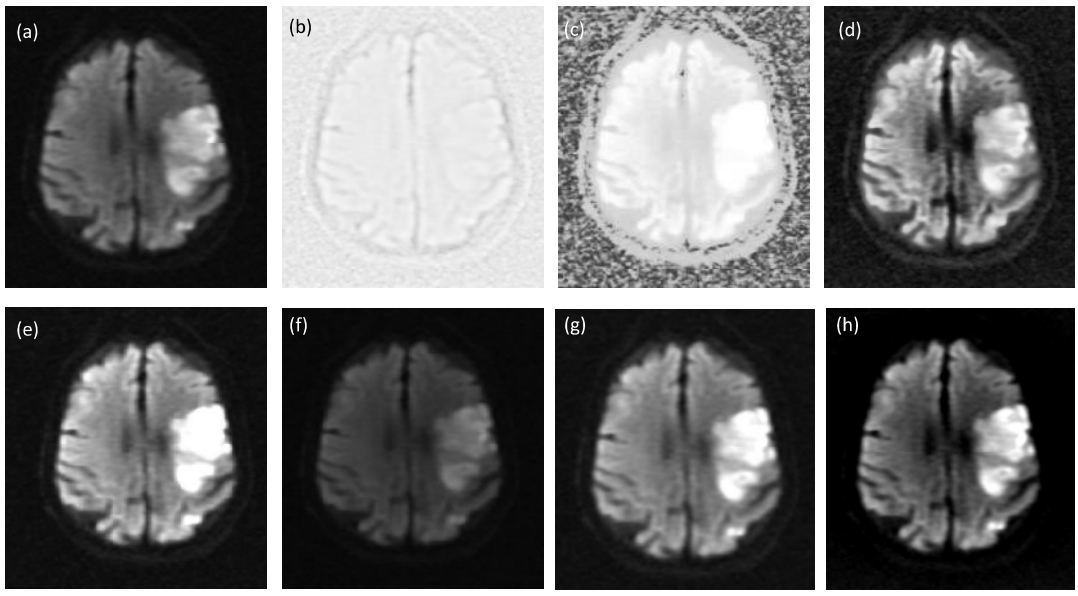

Figure 4-5: Comparative enhancement results of Test 4 (a) Input isotropic DW image (b = 1,000 sec/mm2; repetition time (msec)/echo time (msec) = 3,000/89; matrix, 192 × 192; field of view = 229 × 229 mm, section thickness = 5 mm), image processed using (b) SSR, (c) HE, (d) CLAHE, (e) Gamma (1.2), (f) Gamma (0.9), (g) Photoshop, and (h) proposed algorithm

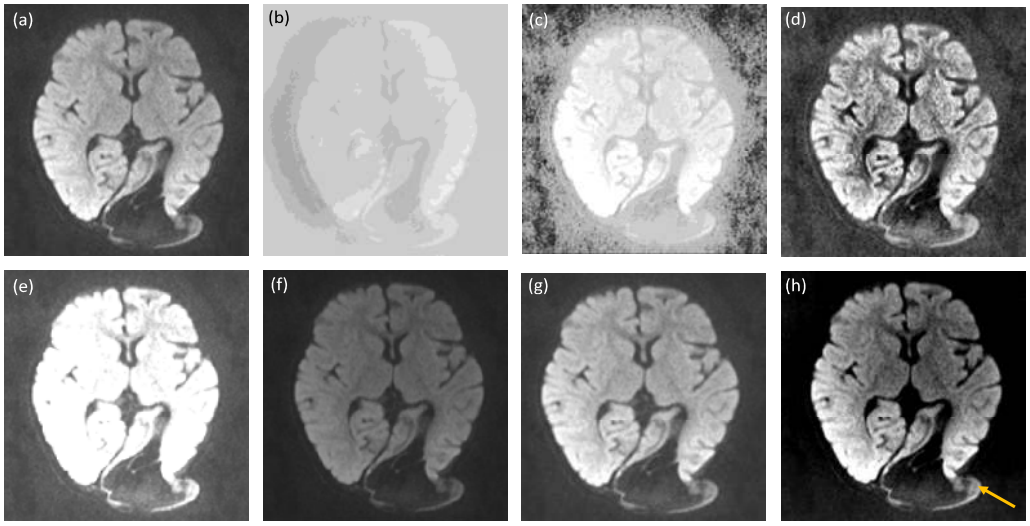

Figure 4-6: Comparative enhancement results of Test 5 (a) Input isotropic DW image (b = 1,000 sec/mm2; repetition time msec/echo time msec = 3,000/89; matrix, 192 × 192; field of view = 229 × 229 mm, section thickness = 5 mm), image processed using (b) SSR, (c) HE, (d) CLAHE, (e) Gamma (1.2), (f) Gamma (0.9), (g) Photoshop, (h) proposed algorithm

Table 4-3: Comparative performance of proposed MO-PSO optimized DSR algorithm with conventional contrast enhancement techniques

Test Image	Performance parameter	Methods					
					Gamma correction		
		SSR	HE	CLAHE	$\Upsilon = 0.9$	$\Upsilon = 1.2$	Proposed Method
Test 3	CEF	0.148	0.581	0.978	0.556	1.938	1.610
	PQM	13.14	9.43	9.49	12.09	9.34	9.84
	MOS	4.998	4.994	4.994	4.999	4.993	4.996
Test 4	CEF	0.515	0.552	1.079	0.554	2.171	1.547
	PQM	11.58	8.23	9.282	10.624	8.772	10.602
	MOS	4.999	4.981	4.993	4.998	4.989	4.998
Test 5	CEF	0.244	0.894	0.847	0.531	1.026	2.224
	PQM	14.40	9.45	10.15	11.21	10.44	10.47
	MOS	4.999	4.994	4.997	4.999	4.998	4.998

Table 4-4: Comparative performance of proposed MO-PSO optimized DSR algorithm with LMMSE filtering followed by conventional contrast enhancement techniques

Filtering Technique	Enhancement Technique	Test 3		Test 4		All tests	
		CEF	PQM	CEF	PQM	CEF	PQM
Rician noise estimation and filtration	SSR	0.132	10.701	0.504	11.787	0.410±0.016	5.705±4.511
	HE	0.448	8.849	0.448	8.849	0.586±0.036	7.845±0.255
	CLAHE	0.822	9.143	0.822	9.143	1.001±0.011	9.159±0.222
	Gamma (Υ= 1.1)	1.602	9.542	1.627	10.624	1.501±0.010	9.455±0.125
Proposed method		1.610	9.840	1.444	9.820	1.603±0.058	9.508±0.116

4.5.2 Optimized modified neuron model of DSR

The two primary signal intensity patterns (i.e., shades of intensity) visible on an MR scan of brain emanate from the cortex-deep nuclei (gray matter) and medulla (white matter). Any departure from this normal signal intensity pattern is perceived as being pathological, and a patterned approach including the distribution and location of such altered signal intensity characteristics along with the overall clinical details forms the basis of imaging-based clinical differential diagnosis [166]. Most of this exercise is done by imaging experts based on their "eye-ball perception" of such shades of gray and rarely if ever actual quantification of screen pixel intensity if relied upon in routine clinical practice. A most algorithm designed to enhance the gray-white matter contrast cause an inadvertent increase in pixel noise as well leading to an overall reduction in image definition. On the other hand, BAT optimization based SR algorithm proposed in the present study is able to achieve an increase in contrast without an attendant increase in the noise.

The experiment started with obtaining Pareto front surfaces of two conflicting image performance metrics F and MOS obtained for MR images: (i) Test 1 implemented on T1 weighted image, (ii) Test 2 implemented on DWI, (iii) Test 3 implemented on FLAIR, and

(iv) Test 4 implemented on T2 weighted. The near optimal solutions are the trade-off between two considered metrics i.e. MOS and F, and vary according to the weight factor (w_k). The chosen sequences of MRI settled for optimum fitness values for different SR parameter are illustrated in Table 4-5.

Table 4-5: Optimized SR parameters and their respective enhancement metrics for different weighting coefficients of Bat optimization

Image	Weight (w_k)	Optimum values of enhancement metrics		SR parameter (for k=0.1)	
		Fitness 1 (MOS)	Fitness 2 (F)	η	Iterations
Test 1	0.17	4.9979	1.1847	2.253	40
	0.33	4.9979	1.1784	2.480	39
	0.50	4.9993	1.1836	2.000	39
	0.67	4.9979	1.1793	2.396	39
	0.83	4.9993	1.1709	2.000	36
	1.00	4.9993	1.1473	2.422	32
Test 2	0.17	4.9925	1.5355	2.489	24
	0.33	4.9924	1.5348	2.094	25
	0.50	4.9925	1.5355	2.500	24
	0.67	4.9926	1.5052	2.191	24
	0.83	4.9922	1.5337	2.000	25
	1.00	4.9973	1.3977	2.170	21
Test 3	0.17	4.9828	1.5013	2.097	24
	0.33	4.9846	1.5033	2.142	24
	0.50	4.9828	1.5343	2.472	24
	0.67	4.9834	1.5349	2.075	25
	0.83	4.9829	1.5344	2.098	25
	1.00	4.9964	1.3161	2.500	25
Test 4	0.17	4.9906	1.4725	2.387	25
	0.33	4.9954	1.4710	2.060	25
	0.50	4.9956	1.4504	2.227	24
	0.67	4.9908	1.4516	2.500	24
	0.83	4.9955	1.4713	2.109	25
	1.00	4.9958	1.3997	2.475	22

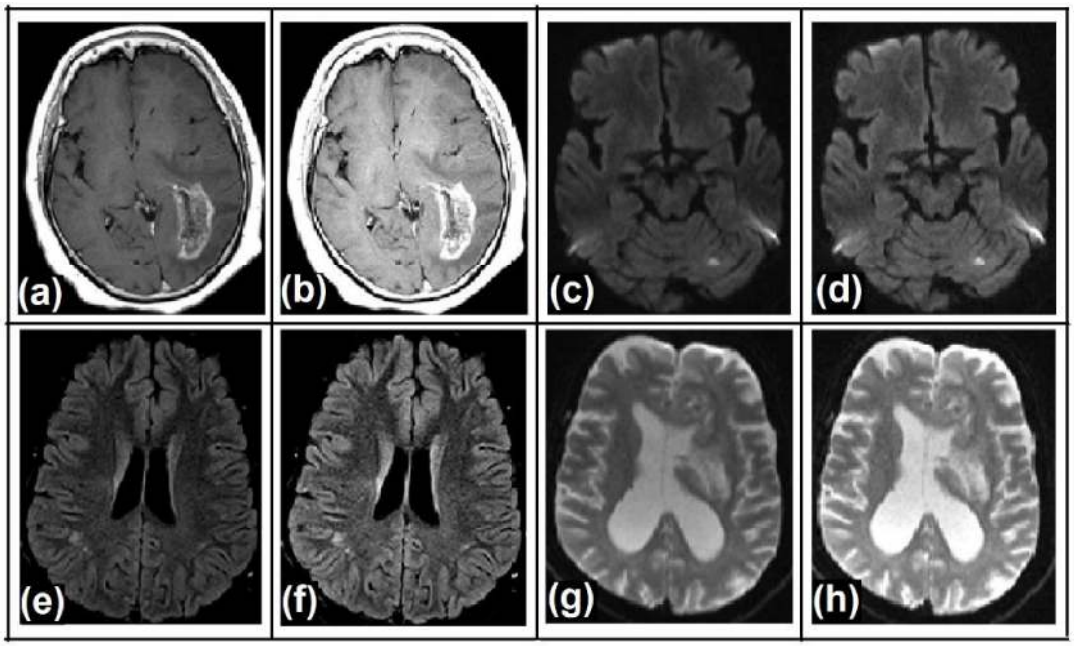

Figure 4-7 Different MRI sequences of abnormal and healthy subjects (a) T1 weighted (Test image 1), (c) DWI (b=1000) (Test image 2), (e) FLAIR (Test image 3), (g) T2 weighted (Test image 4) and (b, d, f and h) respective MOBA optimization based SR processed image

Fig. 4.7 (a, c, e, and g) shows original T1W, DWI (b=1000), FLAIR, and EPI T2W images, whereas the images shown in Fig. 4.7 (b, d, f, and h) are output images corresponding to weight factor of 0.5. Further, we can conclude that for 0.5 value of weight factor we are able to achieve near-optimal results. It can be noted that the enhanced visualization of the left periventricular tumor seen in the post-contrast T1W image in Fig. 4.7 (b), the sensitivity for detection of gadolinium uptake get improved after processing. DWI shown in Fig. 4.7 (c) is a case of lacunar infarct, the white matter hyperintensity is visualized much better with enhanced gray-white matter differentiation in the processed image shown in Fig. 4.7 (d). The processed images in Fig. 4.7 (f and h) are showing better contrast resolution between gray and white matter as compared to the original images. The algorithm produces enhanced gray-

white matter differentiation without an attendant increase in pixel noise. This enhanced gray-white matter differentiation forms a basis of diagnosis of most pathological entities.

4.5.2.1 Case study

The present algorithm has been tested on the two cases: (i) cortical dysplasia (Fig. 4.8) and (ii) mesial temporal sclerosis (MTS) (Fig. 4.9), for these two conditions differential alteration between cortex and medulla is the key to diagnosis. In both these pathologies, the algorithm has been applied to FLAIR sequence, which results in an enhanced gray-white differentiation due to frequency selective suppression of free interstitial water. The subtle diagnostic features could be claimed with confidence only after processing with proposed MO-BA optimization based SR algorithm. The pseudocolored maps of the processed images offered a further advantage as the human eye is known to be more sensitive to minor alteration in the polychromatic spectrum as opposed to that in the monochromatic spectrum in the gray-white range [167]. The supplementary data shows the detailed qualitative comparative analysis among considered de-noising, enhancement and hybrid methods for respective cortical dysplasia and MTS.

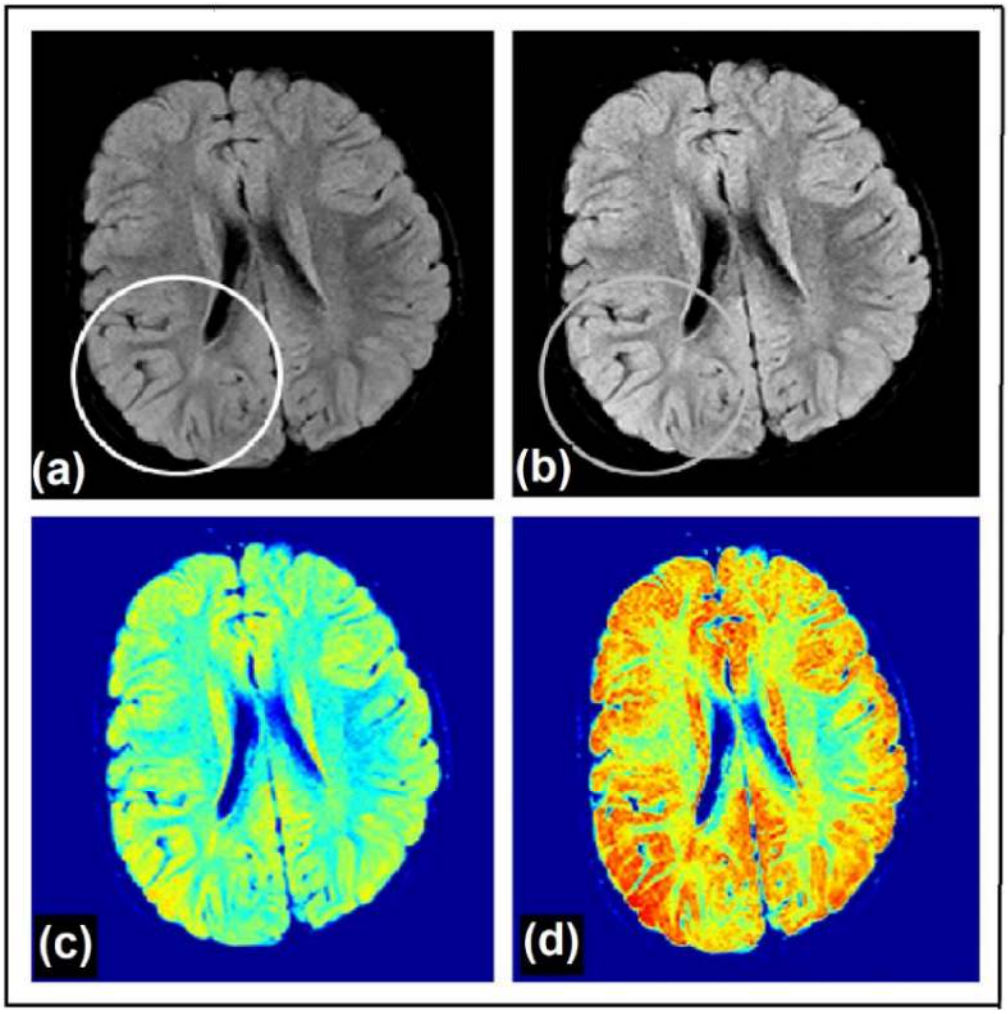

Figure 4-8: Test image 5 (left column) and MO-BA optimized SR processed (right column) axial FLAIR images in a case of right-sided cortical dysplasia showing hyper-intense (bright) signal of the right side parieto-temporal cortex (encircled areas). The gray-white matter differentiation is weak in this region with increased signal intensity due to reduced myelin and organization of cortical architecture apart from the thickened cortex. These changes are seen best in FLAIR images and may be contrasted from the corresponding normal anatomy on left (white circles). Enhancement of these diagnostic features in processed images (gray circle) assists significantly in pick-up during the routine clinical reading of the images. Note the overall change in color hue (red as opposed to yellow) of the cortex in the processed pseudo-colored image has led to a much better gray-white differentiation, in addition, a brighter red hue seen in the pathological area (gray circle) may offer an added advantage for clearly demarcating such areas of disorganized cortical architecture.

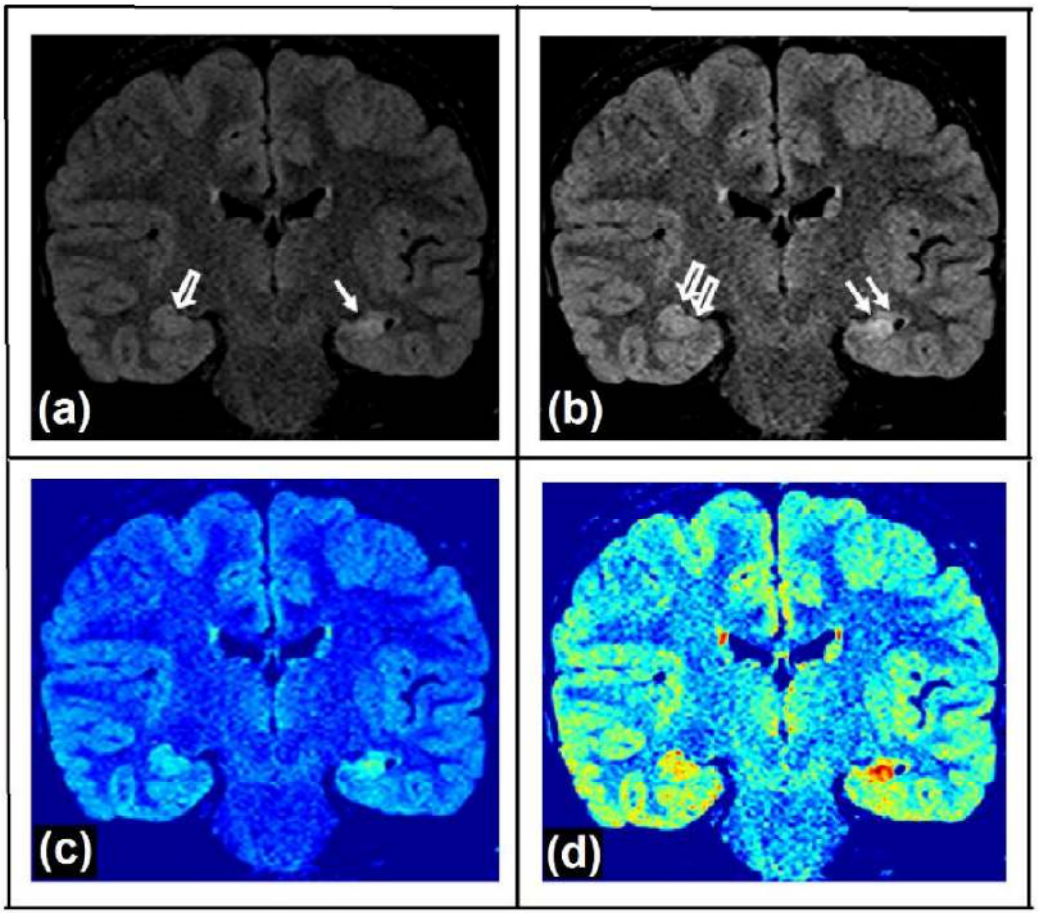

Figure 4-9: Test image 6 (left column) and MO-BA optimized SR processed (right column) coronal FLAIR images in a case of left-sided mesial temporal sclerosis (MTS) showing hyper-intense (bright) signal of the left side hippocampal formation (straight arrow) in comparison to that on the right (open arrow). Such intensity elevation forms the basis of diagnosis in MTS but remains difficult to pick-up by an eye-balling technique in routine clinical practice. The corresponding pseudo-colored image may offer some advantage as is seen in the lower panel, by showing a brighter hue of blue and white on the left side as compared to darker blue only on the right. The signal intensity and color hue difference between the pathological (double straight arrow) and the normal (double open arrow) sides in the processed images is much more convincing. Further, the thickness of the structure in this section (and hence the volume overall) is also reduced on the pathological side, appreciated with increased confidence in processed imaging.

4.5.2.2 Comparative study

The present algorithm has been qualitatively and quantitatively compared with: (i) de-noising using linear minimum mean square error (LMMSE) method [43], (ii) automatic contrast enhancement using contrast limited adaptive histogram equalization (CLAHE) method [164], and (iii) de-noising and contrast enhancement simultaneously using hybridization of LMMSE and CLAHE. Previously, the LMMSE estimator was used to restoring the DWI sequence of MRI, which removes the noise and keep the structural information. As the LMMSE based filtering removes noise from the images and CLAHE increases the contrast, we cascaded both the methods, where CLAHE follows the LMMSE method. The CLAHE and LMMSE based hybrid approach used for tough comparison with the proposed method. The different competitive methodologies have been evaluated in terms of image qualities, i.e. CEF and perceptual quality measure (PQM).

The first row of Fig 4.10 shows the original diffusion-weighted image and processed images, whereas the second row shows the respective pseudocolor images. Fig. 4.10 (b) shows filtered image using the LMMSE method, which reduced the noise, however, produced the blur and there is no enhancement in contrast between the tissues. Fig. 4.10 (c) shows processed image using the CLAHE method, which produced noise and artifacts on the image. The noise and artifact can be easily seen in the respective pseudo color image. Fig. 4.10 (d) shows the image obtained from hybrid (LMMSE followed by CLAHE) approach. This hybrid approach performed better than the LMMSE approach in terms of the contrast between the tissues and performed better than the CLAHE approach in terms of noise. However, artifacts and noise are still present in the output image. On the other hand, there is a good improvement in contrast resolution with the least background noise by using the

proposed algorithm as shown in Fig. 4.10 (e). Further, it can be noted that the visualization of lacunar infarcts in the left posterior limb internal capsule, left lentiform nucleus, and left caudate nucleus are improved (shown in the gray box) as shown in Fig. 4.10 (e). Further subtle lesion in the left cingulate gyrus is detected unambiguously (shown by the white arrow), this was not much clear on the images are shown in Fig. 4.10 (a, b) while labeled as susceptibility artifact on the images shown in Fig. 4.10 (c, d).

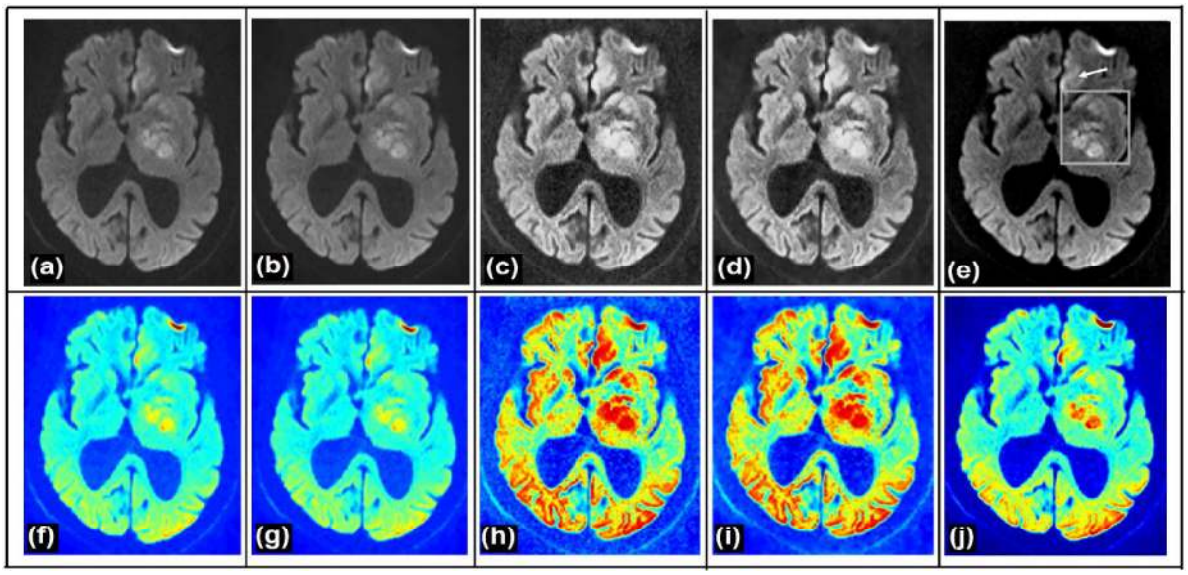

Figure 4-10: Original (a) Test image 7, (b) image filtering using LMMSE method, (c) processed image using CLAHE method (d) processed using LMMSE followed by CLAHE (hybrid), (e) processed image using proposed algorithm and (f-j) respective pseudocolor images

The first row of Fig. 4.11 shows the original T1W image and processed image using LMMSE, CLAHE, hybrid and proposed algorithm respectively from left to right. The second row shows their pseudocolor images. The most optimum contrast resolution is noted in the image achieved using the proposed algorithm in Fig. 4.11 (e). The gray-white matter differentiation is hence the best seen in the latter image making a more conspicuous depiction of the anatomical details, which can be easily seen in its pseudo color image. While the

images are shown in Fig. 4.11 (c and d) also show good contrast resolution, but excess shine through in basal ganglia raise suspicion of para/diamagnetic susceptibility effect (white arrows). On the other hand, the image is shown in Fig. 4.11 (b) has not this problem but offers the poor contrast resolution.

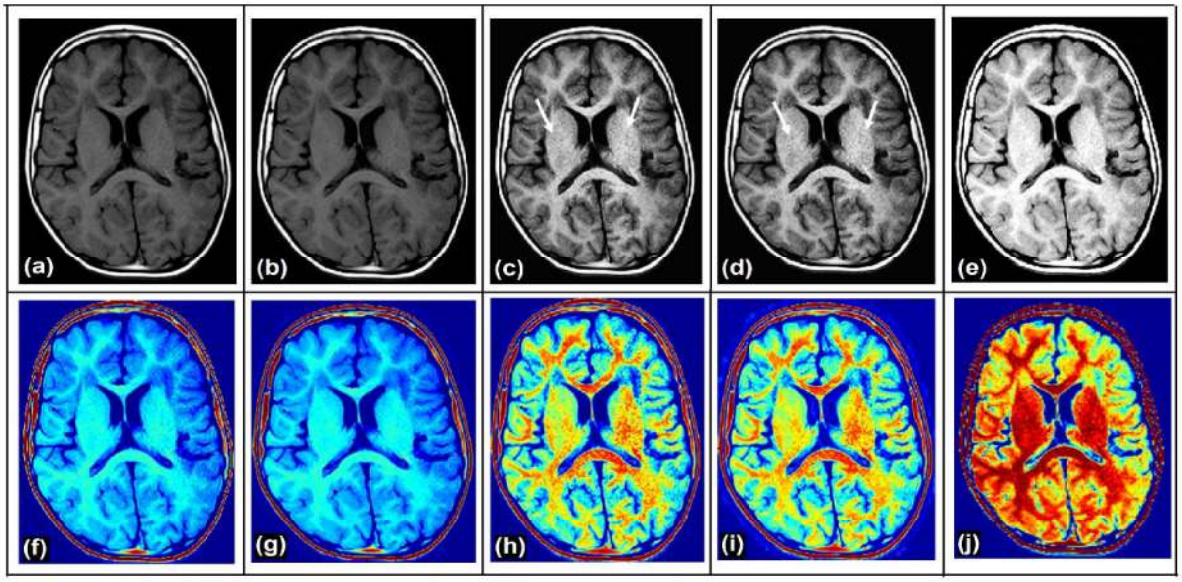

Figure 4-11: Original (a) Test image 8, (b) image filtering using LMMSE Estimator, (c) processed image using CLAHE method (d) processed using LMMSE followed by CLAHE (hybrid), (e) processed image using proposed algorithm and (f-j) respective pseudo color images

Quantitative results in Table 4-6 show that conventional neuron model based algorithm is not capable of enhancing the contrast between the tissues, as $CEF < 1$, whereas LMMSE based method produced insufficient contrast. The CLAHE and hybrid approaches enhanced the contrast but introduced the noise and artifact as observed in Fig. 4.10 and Fig. 4.11. The images processed by the proposed algorithm produce near optimum results with maximum F and second highest PQM as compared to the conventional neuron model for Test image 7 and 8. The value of PQM should be closest to 10 for the best perceptual quality of image [165]. Further, the proposed algorithm was tested and validated for the dataset of more than twenty

test images, which includes DWI, FLAIR, T1 and T2 weighted images. Supplementary results enclosed as 'appendix –B' includes the detailed quantitative comparative analysis for additional images. As discussed earlier, the conventional neuron model based processed images have the best PQM, however, there is poor contrast enhancement between the tissues. The modified SR leads to maximum mean F in comparison to all considered methods and marginally less PQM in comparison to the conventional neuron model based algorithm.

Table 4-6: Quantitative evaluation of proposed MOBA optimized modified SR and other considered methodology

Technique	Test image 7		Test image 8		Image Dataset	
	F	PQM	F	PQM	F	PQM
LMMSE based de-nosing	0.983	9.575	0.972	7.610	1.120 ± 0.200	8.795 ± 0.813
Enhancement using CHAHE	1.135	9.715	0.973	8017	1.292 ± 0.202	7.664 ± 0.594
LMMSE + CHAHE (hybrid)	1.090	9.710	0.973	8.017	1.248 ± 0.166	8.709 ± 0.895
Conventional neuron model	0.940	9.931	0.937	9.770	0.936 ± 0.004	9.513 ± 0.474
Proposed modified model	1.299	9.900	1.047	8.768	1.3312 ± 0.101	8.9620.452

4.5.3 Optimized cascaded model of DSR

The proposed algorithm implemented the cascading of quartic bi-stable and modified potential neuron models. The parameter associated with this cascaded model heuristically searched to achieve optimum image quality with the help of MO-PSO, while considering the maximization of UIQ and contrast enhancement factor (CEF) as the fitness functions. The present study has been carried out in four stages. (i) The experiment shows dominant properties of both DSR models used in proposed cascaded system. (ii) Further, the study investigates the limits of particle search space and controlling parameters associated with the

MO-PSO. (iii) Finally, performed the case study, and (iv) analysis of comparative performance.

First, this study demonstrates the advantage of cascading of two different models of DSR. The variation of CEF and UIQ with respect to the number of iterations for T1 weighted and T2 weighted simulated dataset images have been shown in Fig. 4.12. In this view, the DSR parameters $a, b,$ and λ have been kept fixed with the increase in the number of iterations (please note, at this stage there is no optimization has been performed). As shown in Fig. 4.12 (a) and Fig. 4.12 (c), the image quality CEF keep increasing as increase in the number of iterations for quartic bistable model (n_q), potential neuron model (n_n) and proposed cascaded model of DSR ($n_q + n_n$). However, there is continues decrement in the UIQ as the increment in the number of iterations in case of T2 weighted image, whereas for T1 weighted image UIQ first increase than start decreasing. This analysis suggests that there is a need of a trade-off between these image qualities. Further, Fig. 4.12 demonstrates that the quartic bistable model of DSR perform better than the potential neuron model of DSR for image quality measure CEF, however, lags behind for other image quality measure UIQ. The red line with circle shows in the figures represent the cascading of DSR models gives equitable image quality i.e., unbiased CEF and UIQ.

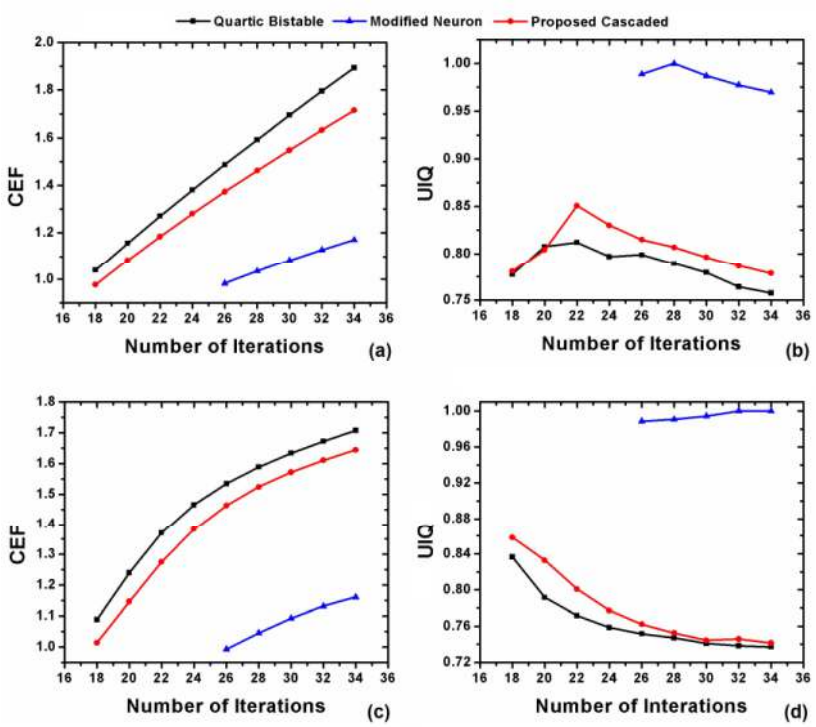

Figure 4-12: Variation of CEF and UIQ index with respect to the number of DSR iterations for (a, b) 80th slice (corrupted with 3% noise) of T1 weighted simulated MRI dataset image, (c, d) 110th slice (corrupted with 3% noise) of T2 weighted simulated MRI dataset image

The variable range of potential neuron model parameter, λ can be derived from the potential curve shown by (2), which preserves the bistable property only for $\lambda\,(t) > 1$; hence, $\lambda\,(t)$ greater than one is an appropriate choice. The present study uses the previously proposed range of quartic bi-stable parameters a and b [136]. The step size used to discretise DSR considered fixed to $k = 0.05$ in this study, which helps to select moderate number of iterations (n) as shown in Fig. 4.12. Please note, the variables a, b, λ *and* n are the particles within the boundary of search space. The particle position initialized randomly in above explained range. The controlling parameter values of PSO selected by initializing the number of iterations 25 and varied number of particles from 10 to 30. The experimental results show that for this fixed number of generations the best results obtained with the population size of

15 for the proposed cascaded model. Further, the number of generations varied by kept fixed population size at 15, it has been observed that best anisotropy obtained with 25 iterations. The other controlling parameters used in this study are illustrated in Table 4-7, where n_q *and* n_n are number of iterations corresponding to quartic bistable model and potential neuron model respectively.

The MO-PSO provides the set of non-dominate solutions called Pareto fronts as shown in Fig. 4.13. The Pareto fronts obtained for two image quality indexes, i.e., CEF and UIQ, whereas the third image quality index, i.e., anisotropy used to pick the dominant solution. Hence, the proposed cascaded DSR based on MO-PSO produces the optimum image based on three image quality indexes. The solution corresponding to the dashed square on the Pareto front surface is a dominant solution. The image generated for this solution is known as an optimized enhanced image, which is shown at the right corner of the Fig. 4.13. The optimized enhanced image has better gray-white matter differentiation in comparison to the input image.

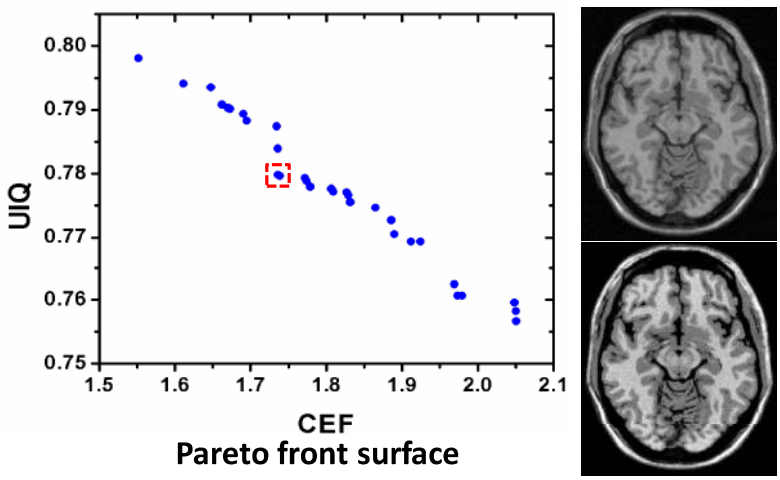

Figure 4-13: Pareto front surface for the 60th slice of simulated T1 weighted MRI dataset image corrupted with 3% noise. Original input image (above) and processed output image (below) corresponding to the solution shown in the red box.

4.5.3.1 Case study

This study considered three pathological cases of different sequences of MRI. The original input images and respective proposed cascaded DSR based on MO-PSO processed images are shown in the first row and second row respectively in Fig. 4.14.

In the first case, Fig. 4.14 (a) shows T1 weighted MRI (resolution 384×512, echo time (TE) 17, repetition time (TR) 1200, field of view (FOV) 180×180) of the neonatal brain. The differentiation between the tissues is accentuated in the processed images, which led to a better gray-white matter differentiation. In second case, Fig. 4.14 (c) shows the lacunar infarct in diffusion-weighted MRI (resolution 192×192, TE 89, TR 3000, FOV 192×192). It can be noted that the better visualization of lacunar infarct has shown in cascaded DSR based on MO-PSO processed image. In the third case, Fig. 4.14 (e) shows FLAIR sequence of MRI (resolution 460×512, TE 3, TR 9000, inversion time (TI) 2500, FOV 200×200) suspected of mesial temporal sclerosis (MST). The hyper-intense region in the hippocampal is the basis of MST diagnosis. The cascaded DSR based on MO-PSO processed image shows higher pixel intensity (arrow) in this region with overall better gray-white matter differentiation in comparison to the input image.

These case studies have shown that the proposed cascaded DSR based on MO-PSO can produce better tissues differentiation and clearer lesions. Further, Table 4-7 shows the quantitative evaluation of the images shown in Fig. 4.14 obtained using the proposed algorithm. The value of CEF higher than one shows that the processed images have better contrast over the input images. The UIQ close to one shows the processed image is well

correlate to the input image. The anisotropy of the processed image is also better than the input image indicates the lesser noise in algorithm processed images.

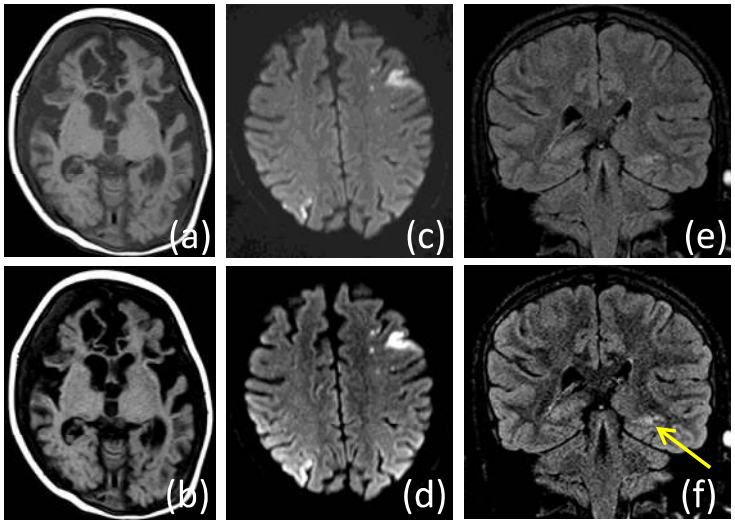

Figure 4-14: (a) Input T1 weighted MRI (Test 1), (b) optimized enhanced image corresponding to Test 1 (DSR parameters a=0.0608, b=5.47×10-9, n_q=23, n_n=15, λ =2.11). (c) Input DWI (Test 2), (d) optimized enhanced image corresponding to Test 2 (DSR parameters: a=0.0466, b=5.62×10-9, n_q=24, n_n=20, λ =2.15). (e) Input FLAIR (Test 3) images, (f) optimized enhanced image corresponding to Test 3 (DSR parameters: a=0.1987, b=6.343×10-9, n_q=24, n_n=24, λ =2).

Table 4-7: Image quality of test images shown in Fig. 4.14 proposed cascaded DSR based on the MO-PSO algorithm

Test image	Anisotropy of input image	Anisotropy of output image	UIQ	CEF
Test 1	0.0064	0.0172	0.74	1.62
Test 2	0.0007	0.0129	0.45	3.41
Test 3	0.0145	0.0153	0.76	1.72

4.5.3.2 Comparative study

This section compares the proposed cascaded DSR based on MO-PSO algorithm with quartic bi-stable DSR based technique and conventional contrast enhancement techniques on T1 weighted and T2 weighted sequences of simulated MRI obtained from BrainWeb dataset.

The MRI images are shown in the first column of Fig. 4.15. are the input images whereas processed images using contrast limited adaptive histogram equalization (CLAHE) method [168], brightness preserving dynamic fuzzy histogram equalization (BPDFHE) based method [169], quartic bi-stable model based DSR [136] and proposed MO-PSO based cascaded DSR approaches are shown in respectively second, third, fourth and fifth columns. The CLAHE processed images are shown in Fig. 4.15 (b, g), this processed image seems to be highly susceptible to noise. The high amount of noise is present on the anatomy of interest and in the background of the processed T2 sequence. The quantitative results in Table 4-8 have shown that the processed images improved the contrast but showing contrast distortion, i.e. low UIQ and low anisotropy in comparison to other methods. BPDFHE algorithm obtained CEF less than one and qualitatively appears ineffective to improve the contrast between the tissues, with lowest UIQ and anisotropy among all considered methods for comparison as shown in Table 4-8. The images produced by quartic bistable based DSR is showing better tissue contrast without increasing the noise. However, the images with best contrast improvement and least distortion were obtained using the proposed MO-PSO based cascaded DSR algorithm. The differentiation between tissues is maximumly accentuated in the image shown in Fig. 4.15 (e, j) the same can be seen in Table 4-8.

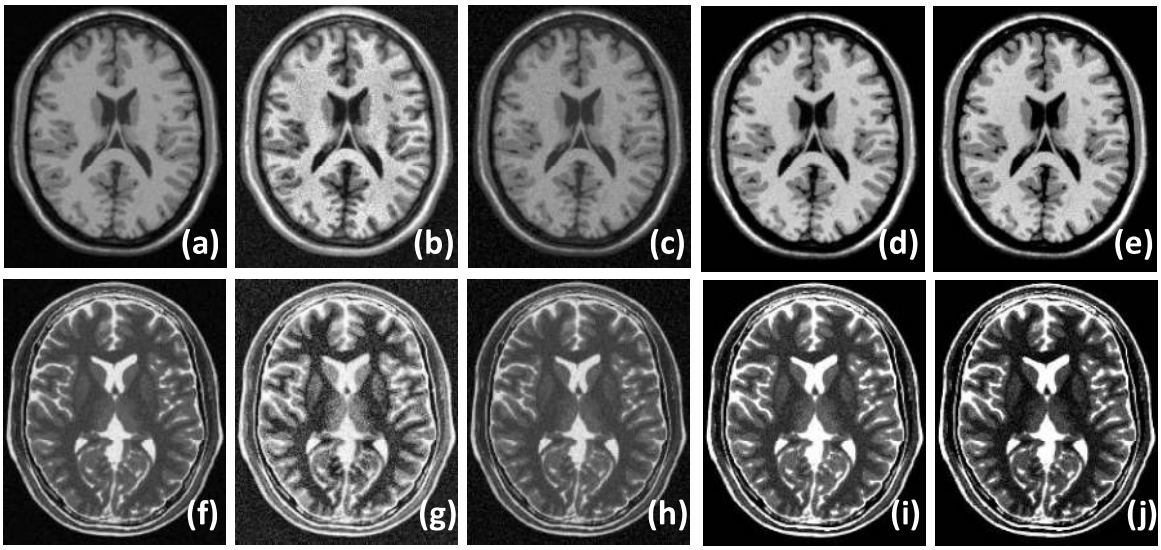

Figure 4-15: (a) Simulated T1 weighted MRI, (b) Simulated T2 weighted MRI, (b,g) processed with CLAHE, (c,h) processed with BPFDHE based algorithm, (d,i) processed with quartic bistable model based DSR, (e,j) processed with proposed MO-PSO based cascaded DSR

Table 4-8: Comparison of proposed cascaded DSR based on MO-PSO and other input parameter independent enhancement methods on ten simulated T1 and T2 weighted dataset images

Enhancement methods	Mean CEF	Mean UIQ	Mean Anisotropy
CLAHE	1.08	0.47	0.013
BPFDHE	0.83	0.73	0.010
Quartic bistable DSR	1.67	0.77	0.020
Proposed algorithm	1.79	0.78	0.021

4.6 Conclusions

The present work proposed optimized quartic bi-stable DSR model, modified neuron model and cascading of modified neuron model and quartic bi-stable model. The parameters associated with DSR have been tuned with the help of optimization algorithms, i.e. MO-PSO and MO-BAT for the maximization of two quality indexes of the MRI data. The multi-

objective optimization has provided the set of non-dominant solutions. The best-enhanced image has been obtained from these solution set by selecting MRI data based on the maximization of another MRI quality measure. As the study has chosen non-referential image quality measures, the algorithm has been found highly useful for the enhancement of real MRI data. The optimum enhancement achieved from the proposed algorithm has improved the diagnosis confidence in case of lacunar infarct and mesial temporal sclerosis. The comparative result has shown that the proposed MO-PSO based cascaded DSR algorithm is capable of producing better enhancement than the quartic bi-stable based DSR, and other conventional enhancement techniques.

5 CHAPTER

ENHANCEMENT AND INTENSITY INHOMOGENEITY CORRECTION OF DIFFUSION-WEIGHTED MR IMAGES OF NEONATAL AND INFANTILE BRAIN

Highlights of the Chapter

- *The data has been segmented according to the mean intensity and PSO based DSR applied to maximize the information within the region and minimize the mean intensity between the different regions*
- *The algorithm has been tested on real Diffusion weighted sequence of neonatal/infantile brain and found highly valuable*
- *The algorithm is capable to reduce the intensity inhomogeneity along with the feature enhancement*

Abstract

Imaging of infantile/neonatal brain mandates tailored radio frequency coils (RF coils) to achieve a homogeneous field over a small region of interest (ROI). Most centers, however, perform pediatric imaging using adult RF coils only as procurement of tailored pediatric coils might prove quite expensive. This practice may not scientifically justified, whereas the image